Article

Contribution of Cations and Anions of Aqueous Electrolytes to the Charge Stored at the Electric Electrolyte/ Electrode Interface of Carbon-Based Supercapacitors

Ivan Aldama, Violeta Barranco, Mirko Kunowsky, Joaquin Ibañez, and Jose M. Rojo

J. Phys. Chem. C, **Just Accepted Manuscript** • Publication Date (Web): 16 May 2017

Contribution of Cations and Anions of Aqueous Electrolytes to the Charge Stored at the Electric Electrolyte/Electrode Interface of Carbon-Based Supercapacitors

by

Ivan Aldama[1], Violeta Barranco[1], Mirko Kunowsky[2], Joaquin Ibañez[3] and Jose M. Rojo[1]*

[1]Instituto de Ciencia de Materiales de Madrid (ICMM); Consejo Superior de Investigaciones Científicas (CSIC); Sor Juana Inés de la Cruz, 3; Cantoblanco; E-28049-Madrid; Spain.

[2]MCMA Departamento de Química Inorgánica; Universidad de Alicante; San Vicente del Raspeig S/N; E-03080-Alicante; Spain.

[3]Centro Nacional de Investigaciones Metalúrgicas (CENIM); CSIC, Av. Gregorio del Amo, 8; E-28040-Madrid; Spain.

*corresponding author: jmrojo@icmm.csic.es

ABSTRACT

For their use in supercapacitors, aqueous electrolytes of acidic (H_2SO_4), neutral (Na_2SO_4, K_2SO_4) and basic (NaOH, KOH) nature are studied, using two microporous binder-free and self-standing carbon cloths as electrodes. The carbon cloths show similar porosities and specific surface areas, but different contents in surface oxygen groups. The working potential window and the specific capacitance associated with the cations and anions are measured. From these parameters, the charges stored by the cations and anions at the electric electrolyte/electrode interface are deduced. The charge stored by the cations is higher than that stored by the anions for the three types of electrolytes. The differences between cations and anions are higher for the acidic and basic electrolyte than for the neutral electrolytes, and also higher for the carbon cloth with the highest content in surface oxygen groups. The charge stored by the cations follows the sequence H_3O^+ > Na^+ or K^+ from the basic electrolytes > Na^+ or K^+ from the neutral electrolytes. The charge stored by the anions follows the sequence SO_4^{2-}>HSO_4^- >OH^-. The results here reported provide a better understanding on the electric double layer of carbon-based supercapacitors. Those results are also of interest for asymmetric and hybrid supercapacitors.

INTRODUCTION

Carbon cloth (CC) or carbon fabric is a self-standing, flexible, light, conductive and porous material suitable as binder-free electrode for supercapacitors, also called electrochemical capacitors.[1-4] The CC, which is usually obtained from carbonization of a woven polymer, consists of woven carbon threads made from bundles of carbon fibers. The self-standing feature makes that CC does not require any binder to be conformed as electrode unlike the powder carbons. Compared with other flexible electrodes such as carbon films consisting of carbide-derived carbons,[5,6] graphene-based materials[7-10] and carbon nanofiber webs,[11] the CC is more flexible and can be folded several times obtaining the same electrochemical behavior.[12, 13] The high flexibility together with the low density (ca. 0.2 g cm^{-3}) makes the CC a promising electrode for flexible/wearable supercapacitors.[13-15] Regarding the electrical conductivity and porosity, the CC shows a sufficient electrical conductivity (in the order of magnitude of 0.1 S cm^{-1}) and a large specific surface area (up to 1000 m^2 g^{-1}). Moreover, the CC is inexpensive.

To improve the specific capacitance of the CCs, several approaches have been tried: (i) Development of larger specific surface areas through activation of the CCs, e.g. by activation of the carbon fibers with CO_2 or KOH or by partial exfoliation of the carbon fibers through chemical or electrochemical oxidation followed by reduction;[16-22] (ii) Doping the carbon fibers with heteroatoms such as O, N, etc. for increasing the pseudocapacitive contribution;[22-25] (iii) Coating the carbon fibers by other carbon materials such as carbon nanotubes or graphene providing an additional capacitance;[26-35] (iv) Coating the carbon fibers by several oxides that contribute with an additional pseudocapacitance; the coating can be obtained by chemical deposition,[36-44] electrochemical deposition[45-47] or printable procedures.[48]

Looking at the electrolytes for carbon-based electrodes, aqueous electrolytes provide higher power densities, but lower energy densities than the organic Et_4NBF_4 electrolyte and the ionic liquid electrolytes.[49-55] Comparing the aqueous electrolytes of acidic, basic and neutral nature in presence of carbon-based electrodes, the working potential window seems to be slightly narrower than 1.0 V for the acidic and basic electrolytes and 1.6-2.2 V for the neutral electrolytes.[56-72] The specific capacitance seems to be higher for the acidic than for the basic electrolyte and higher for the basic than for the neutral electrolyte.[57-61, 63-67, 70, 71] A pseudo capacitance in addition to the double layer capacitance has been reported for the three types of aqueous electrolytes.[57, 58, 61, 63, 67, 73-76] However, the specific capacitance usually reported is the total value, i.e. the specific capacitance due to the combined contribution of the two types of ions, cations and anions, and the working potential window reported is also the total window due to the combined contribution of both, cations and anions. The specific capacitance and the working potential window associated with each ion, cation and anion, are scarcely studied. Such information, however, is important to get a better understanding of the electric electrolyte/electrode interface. The charges stored, i.e. the charges involved in the formation of the double layer plus the charges involved in pseudocapacitive reactions at the electrolyte/electrode interface, are likely very different for the cations and anions, and consequently one of the two types of ions could dominate the total charge stored at the electrolyte/electrode interface. Knowing this information could also be important for asymmetric and hybrid supercapacitors in order to balance the mases of the negative and positive electrodes.

The aim of the present work is to gain understanding on the electrochemical behavior of the three types of aqueous electrolytes (acidic, neutral and basic) in presence of microporous carbon electrodes (two kinds of self-standing carbon cloths

having similar porosities and specific surface areas, but different contents of surface oxygen groups). The potential of zero charge (*PZC*), i.e. the potential at which the same amount of positive and negative charges are located at the electrolyte/electrode interface, was measured and taken as the reference potential for determining the working potential window of the cation and anion.[77-79] The specific capacitances due to the cations and anions were also measured. Taking into account both the working potential windows and the specific capacitances ascribed to the cations and anions, the positive and negative charges stored at the electric electrolyte/electrode interface are estimated under stationary and dynamic conditions for the three types of electrolytes.

EXPERIMENTAL SECTION

Two carbon materials are studied in this work: An original carbon cloth (CC), and a heat-treated one. The original CC is an activated carbon material manufactured by Carbongen SA. The heat-treated CC was obtained in our laboratory from the original CC after heating under N_2 flow of 100 ml min^{-1} at a rate of 5ºC min^{-1}, up to a maximum temperature of 800ºC, which was held for 3 h. Then, the oven was cold down to room temperature while N_2 flowed.

The microstructural characterization was carried out by scanning electron microscopy (SEM) equipped with energy dispersive X-ray spectroscopy (EDS) in a FEG HITACHI S-4800 instrument. The images were obtained in the secondary electron (SE) mode.

Temperature-programmed desorption (TPD) experiments were carried out to characterize the surface chemistry of the carbon cloths by quantifying the evolved CO and CO_2 upon heating. The measurements were performed in TGA equipment (TA Instruments SDT Q600), which was coupled to a quadrupole mass spectrometer

(Balzers Instruments Thermostar GSD 300 T3). For the analysis, approximately 10 mg of the carbon cloth were heated with a ramp of 10 ºC min^{-1} up to 950 ºC in a helium flow of 100 ml min^{-1}.

N_2 and CO_2 adsorption/desorption isotherms were measured with a Micromeritics ASAP 2020. Prior to the adsorption, the carbon cloths were outgassed at 250 ºC for 6 h. Specific surface areas were deduced from Brunauer-Emmett-Teller theory (S_{BET}) and Non-Local Density Functional Theory (S_{DFT}). Volumes of narrow micropores < 0.7 nm ($V_{DR}(CO_2)$) and total volumes of micropores with sizes < 2 nm ($V_{DR}(N_2)$) were calculated, using the Dubinin-Raduskevich method. The volumes of mesopores were deduced from the adsorbed amounts of nitrogen in the range from 0.2 to 0.9 P/P_0.

Electrochemical measurements were performed in three-electrode cells. Circular pieces of the two carbon cloths, of ca. 12 mm in diameter and 0.5 mm thick were punched out. The weights of the original CC and heat-treated CC were ca. 12 and 9 mg, respectively. These circular pieces were used as working electrodes. A platinum wire was the counter electrode. The reference electrodes were: (i) Hg/Hg_2SO_4 for the acidic electrolyte 2M H_2SO_4, (ii) Ag/AgCl for the neutral electrolytes 1M Na_2SO_4 and 1M K_2SO_4, and (iii) Hg/HgO for the basic electrolytes 1M NaOH and 1M KOH. In some particular cases, symmetric two-electrode cells were assembled. The two equal pieces of the carbon cloth were separated by a glassy microfiber paper (Whatman 934 AH). Prior to all the electrochemical measurements, the CCs were immersed into the electrolyte under primary vacuum (ca. 10^{-1} Torr) for 2 h.

RESULTS and DISCUSSION

Two carbon materials were used as electrodes in this work, an original carbon cloth (CC), and a heat-treated one. The SEM images revealed that the original CC is made from woven threads (Figure 1a), which consisted of bundles of ca. 600 carbon

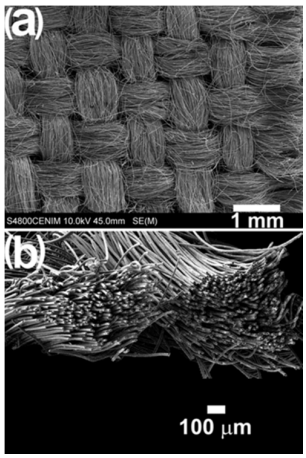

Figure 1. SEM pictures showing a piece of the original carbon cloth (a) and two threads consisting of bundles of carbon fibers (b).

fibers (Figure 1b). Each carbon fiber had 6-7 μm in diameter (Figure 2a). Despite the anisotropy of the carbon fibers along and across the fiber axis (Figure 2a), their interior looked rather isotropic and consisted of connected carbon particles of 15-30 nm size (Figure 2b). Voids appeared between the carbon particles and were of similar size as the

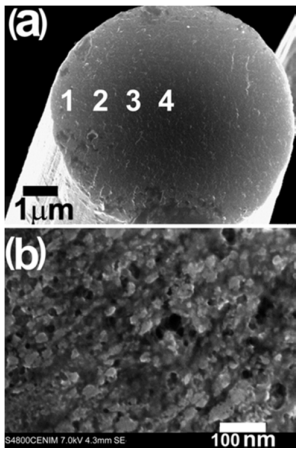

Figure 2. SEM picture of the section of a carbon fiber (a) and a magnified picture of that section (b).

carbon particles themselves, from 15 to 30 nm. The presence of these voids could favor the infiltration of the electrolyte into the carbon fibers. In order to confirm this, the section of a carbon fiber that had been infiltrated with the KOH electrolyte was analyzed by EDS. The results revealed that the potassium content was nearly the same at the outer part (marked as 1 in Figure 2a) and at the inner part (marked as 4 in that Figure) of the carbon fiber; the EDS results are outlined in Table S1. The morphology of the heat-treated CC was similar to that of the original CC (not shown).

The amounts of evolved CO and CO_2, which originated from the oxygen groups at the surface of the two carbon cloths, were deduced by TPD. The results shown in Table 1 reveal that the CO and CO_2 content of the heat-treated CC are 3 and 4 times lower, respectively, as compared with the original CC. These strong decreases indicate that the surface oxygen groups of the original CC were efficiently removed after heating under N_2 flow.

Table 1. Contents of CO and CO_2 deduced from TPD measurements, total micropore volume ($V_{DR}(N_2)$), narrow micropore volume ($V_{DR}(CO_2)$), supermicropore volume ($V_{DR}(N_2)$- $V_{DR}(CO_2)$), mesopore volume (V_{Meso}) and specific surface areas deduced from DFT (S_{DFT}) and BET method (S_{BET}).

Electrode	CO µmol g^{-1}	CO_2 µmol g^{-1}	$V_{DR}(N_2)$ cm^3g^{-1}	$V_{DR}(CO_2)$ cm^3g^{-1}	$V_{DR}(N_2)$- $V_{DR}(CO_2)$ cm^3g^{-1}	V_{Meso} cm^3g^{-1}	S_{DFT} m^2g^{-1}	S_{BET} m^2g^{-1}
Original CC	3253	1009	0.526	0.258	0.268	0.032	944	1047
Heat-treated CC	1122	248	0.696	0.265	0.431	0.038	972	1241

The N_2 and CO_2 adsorption isotherms of the original and the heat-treated CC are shown in Figure 3. For the N_2 adsorption isotherms of both samples (Figure 3a), the adsorbed volume sharply increases at relative pressures below 0.1, followed by a slight increase in adsorbed volume at relative pressures between 0.2 and 0.9. The former feature is ascribed to micropores, i.e. pores with sizes <2 nm, while the latter feature is

ascribed to mesopores, i.e. pores with sizes in the range 2-50 nm. The CO_2 adsorption isotherms (Figure 3b) show similar shapes and both carbon cloths adsorb similar

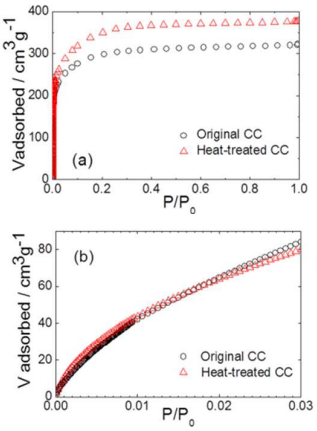

Figure 3. N_2 (a) and CO_2 (b) adsorption isotherms of the original (circles) and heat-treated (triangles) CC.

volumes. The textural results are shown in Table 1. The slight increase of the specific surface areas, S_{BET} and S_{DFT}, (19 % and 3 % , respectively) and the total micropore volume, $V_{DR}(N_2)$, (24 %) from the original to the heat-treated CC are mainly associated with the decrease in weight (ca. 20 %) rather than with the development of additional pores upon the heating. The values for the volume of narrow micropores with sizes <0.7 nm, $V_{DR}(CO_2)$, and mesopores, V_{Meso}, are similar for the two samples. The largest difference between the two samples is found for the wider micropores, also called supermicropores, with sizes in the range of 0.7-2 nm, which are calculated by $V_{DR}(N_2)$ - $V_{DR}(CO_2)$. This result agrees with (i) the pore size distribution deduced from the DFT and shown in Figure S1 and (ii) the fact that the average size of all pores is similar for the two carbon cloths, 1.8 nm for the original CC and 1.9 nm for the heat-treated one. Therefore, the heat treatment, and the corresponding removal of surface oxygen groups, leads to a slight generation of new porosity, mostly in the micropore range from 0.7 to 2 nm, and also, to a slight increase of the specific surface area.

In the literature, sometimes the sulfuric acid is reported to be dissociated in aqueous solutions with SO_4^{2-} and H_3O^+ as the dominant ions. However, the sulfuric acid dissociates in water in two steps. In the first step, sulfuric acid is completely transformed into bisulfate (HSO_4^-) ions and hydronium (H_3O^+) ions. In the second step, the bisulfate ions are partially transformed into sulfate (SO_4^{2-}) ions and H_3O^+ ions, according to the equilibrium constant $K_a=10^{-1.99}$. Therefore, the dominant ions in the aqueous solution are HSO_4^- and H_3O^+. Sodium sulfate (Na_2SO_4) and potassium sulfate (K_2SO_4) dissociate completely in water into the cations Na^+ and K^+, respectively, and the anion SO_4^{2-}. Sodium hydroxide (NaOH) and potassium hydroxide (KOH) dissociate completely in water into the cations Na^+ and K^+, respectively, and the anion OH^-. The main drawbacks of the neutral electrolytes as compared with the acidic and basic electrolytes are their lower ionic conductivity and their higher freezing temperature close to 0 ºC;[80] the latter limits their use at temperatures above 0ºC.

The cyclic voltammetry (CV) measured for the cations (cathodic side) and anions (anodic side) of an acidic (H_2SO_4), a neutral (Na_2SO_4) and a basic (KOH) electrolyte, using the original CC are shown in Figure 4 as examples. The total CV, *i.e.*

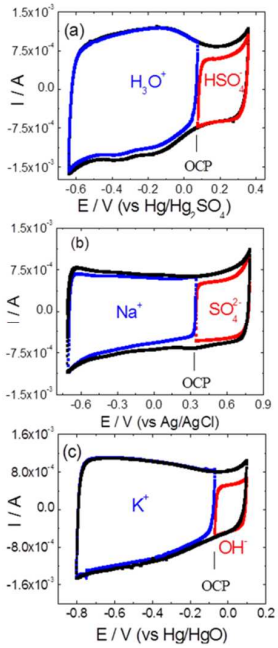

Figure 4. Cyclic voltammetries recorded for the electrolytes: H_2SO_4 (a), Na_2SO_4 (b) and KOH (c) on the original CC. The voltage scan rate was 0.5 mV s^{-1}.

the CV recorded in the total potential window comprising the cathodic and anodic response, is also shown for the three electrolytes. The significant increase in intensity at very negative potentials and at very positive potentials is associated with water electrolysis, the former causing hydrogen evolution and the latter oxygen evolution. From the CV measurements, the lowest cathodic potential, the highest anodic potential and the total potential window were determined. The CVs also provide information about the open circuit potential (*OCP*) for each electrolyte; the *OCP* is refereed to Hg/Hg_2SO_4 for the acidic electrolyte, to Ag/AgCl for the neutral electrolytes and to Hg/HgO for the basic electrolytes. However, all the *OCP*s, and hence all potentials, can be referred to the standard hydrogen electrode (SHE). The CVs associated with the anions HSO_4^-, SO_4^{2-} and OH^- show rectangular shapes that are characteristic for the double layer capacitance. The CVs associated with the cations H_3O^+, Na^+ and K^+ show humps that are characteristic for a pseudo capacitance, in addition to the double layer capacitance.[57, 58, 61, 63, 67, 73-76] The humps are more noticeable for the cations of the acidic and basic electrolytes than for those of the neutral electrolyte.

The total specific capacitance, C_{total}, i.e. the specific capacitance measured in the total potential window, and the specific capacitance associated with the cations, C_+, and anions, C_-, measured in the cathodic and anodic potential range, respectively, were determined from galvanostatic measurements at 1 mA cm^{-2}, i.e. under stationary conditions (see Figure 5 as an example, using the sulfuric acid electrolyte with the original CC). The three specific capacitances were determined according to $C=I\cdot t/\Delta V\cdot m$, where I is the current applied, t is the time for the discharge in Fig. 5a and the time for the electro-desorption "des" in Figs. 5b and 5c, ΔV is the potential range and m is the

weight of the carbon cloth. The *OCP*, which is affected by the surface chemistry of the electrode, cannot be taken as the reference potential. However, the potential of zero

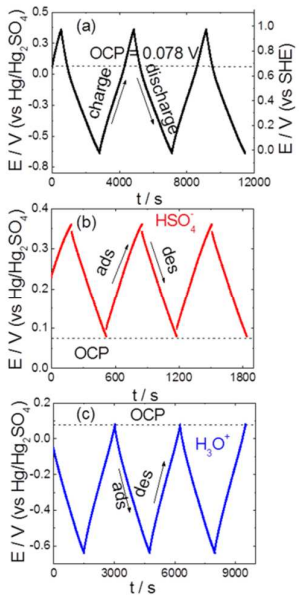

Figure 5. Galvanostatic charge/discharge plots recorded for the sulfuric acid electrolyte on the original CC in the total voltage range (a) and in the partial voltage ranges from the *OCP* to positive voltages (b) and to negative ones (c). The three plots were obtained at 1 mA cm^{-2}.

charge (*PZC*), which is the potential when the same amount of positive and negative charges are located at the electrolyte/electrode interface, is the reference potential taken to determine the potential ranges for the cations and anions. The potential range from the *PZC* to the lowest potential at the onset of the hydrogen evolution is the potential range for the cation, ΔV_+. The potential range from the *PZC* to the highest potential at the onset of the oxygen evolution is the potential range for the anion, ΔV_-. The parameters *PZC*, ΔV_+ and ΔV_- were measured for each electrolyte in presence of the two carbon cloths.

To determine the *PZC* value, the impedance plot *-Z"* vs. *Z'* was recorded at certain potentials in a broad potential range, from potentials below the *OCP* to potentials above the *OCP*. Figure 6a shows the impedance plot obtained for the H_2SO_4

electrolyte and the original CC as an example. Between 1 and 15 mHz, the vertical line is ascribed to the capacitive response. Above 15 mHz, a small arc is also observed (inset

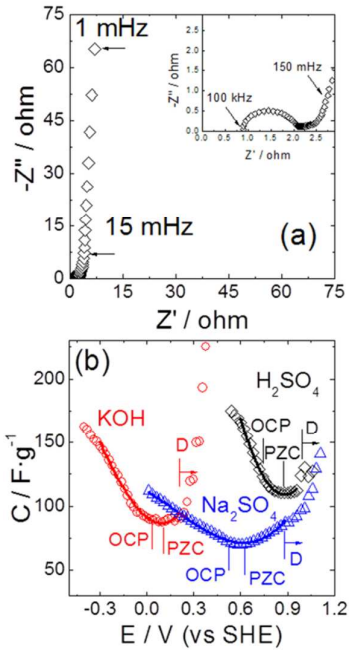

Figure 6. (a) Impedance plot recorded for the H_2SO_4 electrolyte at the *OCP* value on the original CC. Inset: the magnified plot obtained at higher frequencies. (b) Variation of the specific capacitance measured at 1 mHz vs. the potential for three electrolytes, KOH, Na_2SO_4 and H_2SO_4, in presence of the original CC. Solid lines are the best fittings for determining the *PZC*.

of Figure 6a). At the lowest frequency of 1 mHz the imaginary impedance is much higher than the real impedance and the real capacitance, *C*, can be estimated according to $C=-1/(Z''\cdot\omega)$; where $-Z''$ is the value of the imaginary impedance and $\omega=2\cdot\pi\cdot\nu$, ν is the frequency expressed in hertz. The dependence of the real *C* measured at 1 mHz as a function of the potential, *E*, is shown for the three electrolytes, using the original CC (Figure 6b). To compare the three plots, the potentials were referred to the SHE. For each electrolyte, the *OCP* and the potential at the onset of the oxygen evolution (*D*) are marked. The potential at the onset of the hydrogen evolution was not attained. For the three electrolytes, *C* decreases first with the increase of *E* and then increases showing a minimum. The *PZC* is the potential determined at that minimum. For potentials below

PZC the capacitance is dominated by the cations. For potentials above *PZC* the capacitance is dominated by the anions.[77-79] The potential at the minimum was obtained from the fitting of the experimental $C(E)$ data to a polynomic equation (Figure S2).

Tables 2 and 3 summarize the values of *OCP*, *PZC*, ΔV_+, ΔV_- and ΔV_{total} obtained for each electrolyte in presence of the original and heat-treated CC, res-

Table 2. The original carbon cloth in presence of several electrolytes. The open circuit potential (*OCP*), potential of zero charge (*PZC*), working potential window for the cation (ΔV_+) and for the anion (ΔV_-) from the *PZC*, and the total working potential window (ΔV_{total}). The total specific capacitance measured (C_{total}) and the specific capacitance measured for the cation (C_+) and for the anion (C_-). The specific capacitance ($C_{cal\ total}$) calculated according to equation (1), and the charges due to the cations (Q_+) and anions (Q_-) calculated according to the equations (2), (4) and (3), (5), respectively.

Electrolyte	*OCP* V	*PZC* V	ΔV_+ V	ΔV_- V	ΔV_{total} [d] V	C_{total} F g^{-1}	C_+ F g^{-1}	C_- F g^{-1}	$C_{cal\ total}$ F g^{-1}	Q_+ C g^{-1};%	Q_- C g^{-1};%
H_2SO_4	0.078[a] ±0.001	0.230[a] ±0.020	0.840	0.100	0.94	187 ±10	192 ±10	109 ±7	183 ±9	161; 93 ±9;±5	11; 7 ±1;±1
Na_2SO_4	0.330[b] ±0.001	0.408[b] ±0.020	0.808	0.372	1.18	106 ±11	107 ±11	91 ±9	102 ±13	86; 72 ±9;±8	34; 28 ±4;±6
K_2SO_4	0.330[b] ±0.001	0.436[b] ±0.020	0.836	0.304	1.14	105 ±10	104 ±10	97 ±9	102 ±11	87; 75 ±9;±8	29; 25 ±3;±5
NaOH	-0.063[c] ±0.001	0.040[c] ±0.020	0.840	0.010	0.85	138 ±8	139 ±8	70 ±7	138 ±7	117; 99 ±7;±5	1.0; 1 ±0.2;±1
KOH	-0.068[c] ±0.001	0.034[c] ±0.020	0.779	0.121	0.90	140 ±7	149 ±7	67 ±7	138 ±7	116; 93 ±6;±5	8; 7 ±1;±1

[a] *OCP* vs Hg/Hg_2SO_4; [b] *OCP* vs Ag/AgCl; [c] *OCP* vs Hg/HgO; [d] $\Delta V_{total} = \Delta V_+ + \Delta V_-$

Table 3. The heat-treated carbon cloth in presence of several electrolytes. The open circuit potential (*OCP*), potential of zero charge (*PZC*), working potential window for the cation (ΔV_+) and for the anion (ΔV_-), and the total working potential window (ΔV_{total}) . The total specific capacitance measured (C_{total}) and the specific capacitance measured for the cation (C_+) and for the anion (C_-). The specific capacitance ($C_{cal\ total}$) calculated according to equation (1), and the charges due to the cations (Q_+) and anions (Q_-), calculated according to the equations (2), (4) and (3), (5), respectively.

Electrolyte	*OCP* V	*PZC* V	ΔV_+ V	ΔV_- V	ΔV_{total}[d] V	C_{total} F g^{-1}	C_+ F g^{-1}	C_- F g^{-1}	$C_{cal\ total}$ F g^{-1}	Q_+ C g^{-1};%	Q_- C g^{-1};%
H_2SO_4	-0.010[a] ±0.001	-0.027[a] ±0.030	0.613	0.327	0.94	150 ±8	154 ±8	122 ±6	143 ±7	94; 70 ±5;±4	40; 30 ±2;±3
Na_2SO_4	0.190[b] ±0.001	0.145[b] ±0.030	0.745	0.455	1.20	109 ±10	105 ±10	111 ±7	107 ±10	78; 61 ±8;±6	51; 39 ±3;±6
KOH	-0.082[c] ±0.001	-0.004[c] ±0.030	0.746	0.104	0.85	128 ±9	132 ±9	77 ±8	125 ±8	98; 92 ±7;±7	8; 8 ±1;±1

[a] *OCP* vs Hg/Hg_2SO_4; [b] *OCP* vs Ag/AgCl; [c] *OCP* vs Hg/HgO; [d] $\Delta V_{total} = \Delta V_+ + \Delta V_-$

pectively. The values of *PZC* are different from those of *OCP*, especially for the acidic electrolyte and the original CC, the latter with the highest content of surface oxygen groups. In the case of all possible electrolyte/electrode combinations, ΔV_+ is higher than ΔV_-. The difference between ΔV_+ and ΔV_- is more important for the acidic electrolyte and the basic electrolytes than for the neutral ones. Comparing the two carbon cloths, the difference between ΔV_+ and ΔV_- is higher for the original CC than for the heat-treated one. The values of ΔV_+ are similar for the three types of electrolytes. However, the values of ΔV_- are higher for the neutral electrolytes than for the acidic electrolyte and the basic electrolytes. The total potential window, defined as $\Delta V_{total}=\Delta V_+ + \Delta V_-$, is broader for the neutral electrolytes than for the acidic and basic electrolytes. These results agree with those reported by other authors.[64, 66, 70, 71] However, it is worth to note that ΔV_{total} is affected by the potential scan rate or the current density chosen for the electrochemical measurements. While the ΔV_{total} value was of 1.6 V as measured at 10 mV s^{-1} for the Na_2SO_4 electrolyte in presence of the original CC, the ΔV_{total} narrowed to 1.2 V as measured at 0.2 mV s^{-1} (Figure S3). To avoid any side reaction associated with water electrolysis, the ΔV_{total} value taken in this work for the neutral electrolytes was 1.2 V. This value is lower than that reported in other papers for neutral electrolytes.[66,70]

Tables 2 and 3 also summarize the values measured for C_+, C_- and C_{total} for each electrolyte in presence of the two carbon cloths. For all possible electrolyte/electrode combinations, the values of C_+ are higher than those of C_-. The difference between C_+ and C_- is higher for the original CC, with higher content of surface oxygen groups and slightly smaller surface area, than for the heat-treated CC. These results agree with a pseudocapacitive contribution to the C_+ value; the pseudocapacitive contribution is higher for the acidic electrolyte than for the basic one and higher for the original CC than for the heat-treated one as shown in Table S3. From the point of view of the double layer capacitance, the minimum size of the electro-adsorbed H_3O^+, K^+ and Na^+ is 0.4-0.5 nm and that of the electro-adsorbed HSO_4^-, SO_4^{2-} and OH^- is 0.5-0.65 nm.[56, 81-84] Hence, the surface area available for the electro-adsorbed cations should be larger than that available for the electro-adsorbed anions. Comparing the values of C_+, they follow the trend H_3O^+ > Na^+ or K^+ from the basic electrolytes > Na^+ or K^+ from the neutral electrolytes. This trend can be explained on the basis of (i) the contribution of the pseudo capacitance according to the trend acidic>basic>neutral electrolyte and (ii) the similar contribution of the double layer capacitance according to the similar sizes of the electro-adsorbed cations. The specific capacitance C_- is ascribed to a double layer contribution only as already discussed. The values of C_- follow the trend HSO_4^-≈SO_4^{2-} >OH^-. These results agree with the smaller size of the electro-adsorbed bisulfate and sulfate ion, of ca. 0.5 nm, [56,82,84] as compared with the size of the electro-adsorbed hydroxyl ion, of 0.63 nm, [83] and hence with a larger surface area available for the bisulfate and sulfate ion. Comparing C_- for the two carbon cloths, the values of C_- are slightly higher for the heat-treated CC with slightly broader micropores and larger surface area. The measured total specific capacitance, C_{total}, is higher for the acidic electrolyte than for the basic electrolytes, the neutral electrolytes showing the lowest

values. These results agree with those reported by other authors.[57-61, 63-67, 70, 71] Comparing the two carbon cloths, no appreciable differences of C_{total} are found for the neutral electrolytes. When acidic and basic electrolytes are compared, higher C_{total} values are measured for the original than for the heat-treated CC, despite the slightly larger surface area of the latter. These results agree with the higher pseudocapacitive contribution of the cations for the original CC (Table S3).

In this work, the total specific capacitance is calculated, $C_{cal\ total}$, according to the equation:

$$C_{cal\ total} = (C_+ \cdot \Delta V_+ + C_- \cdot \Delta V_-)/(\Delta V_+ + \Delta V_-) \quad (1)$$

Where C_+ and ΔV_+ are associated with the cation and C_- and ΔV_- are associated with the anion. The values of $C_{cal\ total}$ (Tables 2 and 3) agree with those of C_{total}, experimentally measured in the three-electrode cell, confirming the validity of eq. (1). Therefore, during the discharge in the total potential range, first the anions are electro-desorbed and then the cations are electro-adsorbed together with pseudocapacitive redox reactions. During the charge, first the cations are electro-desorbed together with the return of pseudocapacitive redox reactions and then the anions are electro-adsorbed (Figure 5 a). The experimental specific capacitances, C_{2E}, were also obtained from galvanostatic measurements in symmetric two-electrode cells according to $C_{2E} = 2 \cdot I \cdot t_d / \Delta V \cdot m$, where the parameter I, t_d and ΔV have the meaning already discussed and m is the mass of one electrode only (Figure S4). The experimental values of C_{2E} agree with those of C_{total}. Thus, C_{total} shows the values of 187, 140 and 106 F g^{-1} and C_{2E} shows the values of 178, 144 and 99 F g^{-1} for the acidic H_2SO_4, basic KOH and neutral Na_2SO_4 electrolyte, respectively, with the original CC. The agreement between $C_{cal\ total}$, C_{total} and C_{2E} shows that electro-adsorption/desorption of cations and anions together with pseudocapacitive reactions of the cations are involved in each electrode of the symmetric two-electrode

cell, and hence the two ions contribute to the capacitance of each electrode, C_E, according to $1/C_{2E} = 1/C_E + 1/C_E$. This interpretation differs from the one, which assumes that only one type of ion, either cation or anion, is involved in each electrode of the symmetric two-electrode cell, and hence $1/C_{2E} = 1/C_+ + 1/C_-$. This equation, sometimes used, differs clearly from eq. (1).

Based on the validity of eq. (1), the specific charges stored by the cations (Q_+) and anions (Q_-) at the electric electrolyte/electrode interface can be estimated according to:

$$Q_+[\mathrm{C/g}] = C_+ \cdot \Delta V_+ \quad (2)$$

$$Q_-[\mathrm{C/g}] = C_- \cdot \Delta V_- \quad (3)$$

where Q_+ and Q_- are expressed in Coulombs per gram.

The relative charges stored by the cations (Q_+) and the anions (Q_-) can be estimated according to the equations:

$$Q_+[\%] = [C_+ \cdot \Delta V_+ / (C_+ \cdot \Delta V_+ + C_- \cdot \Delta V_-)] \cdot 100 \quad (4)$$

$$Q_-[\%] = [C_- \cdot \Delta V_- / (C_+ \cdot \Delta V_+ + C_- \cdot \Delta V_-)] \cdot 100 \quad (5)$$

where Q_+ and Q_- are expressed in percentages.

In the following, the charges Q_+ and Q_- are compared with each other for the three types of electrolytes and the two carbon cloths (Tables 2 and 3). The values of Q_+ are much higher than those of Q_- for all the electrolytes independent of the carbon cloth chosen. As an example, they can reach the values of 161 C g^{-1} for H_3O^+ vs. 11 C g^{-1} for HSO_4^- with the original CC and 94 C g^{-1} for H_3O^+ vs. 40 C g^{-1} for HSO_4^- with the heat-treated CC. The higher values of Q_+ as compared with to those of Q_- come from two facts: (i) C_+ is higher than C_- and (ii) ΔV_+ is broader than ΔV_-. Therefore, the cations dominate the charge involved at the electric electrolyte/electrode interface for the three types of electrolytes with the two carbon cloths. It suggests the preferential use of the

two carbon cloths as negative electrodes in asymmetric and hybrid supercapacitors. The values of Q_+ follow the trend H_3O^+ (from the acidic electrolyte) > Na^+ or K^+ (from the basic electrolyte) > Na^+ or K^+ (from the neutral electrolyte) for the original CC and the trend $H_3O^+ \approx K^+$ (from the basic electrolyte) > Na^+ (from the neutral electrolyte) for the heat-treated CC. Owing to ΔV_+ is similar for all the cations in a given CC, the differences found in Q_+ come from the different values of C_+. Comparing each cation for the two carbon cloths, the value of Q_+ is higher for the original CC due to its slightly higher values of C_+ and ΔV_+. The slightly higher C_+ values are associated with the presence of a pseudocapacitive contribution, which is higher for the original CC as already discussed. The values of Q_- follow the trend SO_4^{2-} > HSO_4^- > OH^- for the two carbon cloths. Despite the SO_4^{2-} anion shows values of C_- slightly lower than those of HSO_4^-, the former anion shows values of ΔV_- clearly higher; it explains why Q_- for the SO_4^{2-} anion is higher than for the HSO_4^- one. The OH^- anion shows lower values of both C_- and ΔV_-, and consequently Q_- is lower. Comparing each anion for the two carbon cloths, the value of Q_- is higher for the heat-treated CC due to its slightly higher values of C_- and ΔV_-. The slightly higher values of C_- seem to be associated with the slightly larger surface area of the heat-treated CC.

Finally, the charges stored under dynamic conditions are studied through the dependence of C_+ and C_- against the current density (Figure 7). For the three types

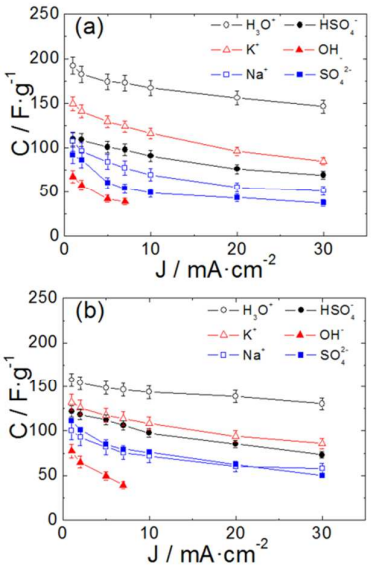

Figure 7. Dependence of the specific capacitance associated with the cations and anions of the electrolytes H_2SO_4, Na_2SO_4 and KOH as a function of the current density for the original (a) and heat-treated (b) CC.

of electrolytes and the two carbon cloths, C_+ and C_- decrease with the increase of the current density; however, the capacitance retention depends on the type of ion and also on the selected carbon cloth (Table 4). The capacitance retention of the cations follows the trend H_3O^+ (from the acidic electrolyte) > K^+ (from the basic electrolyte) ≥ Na^+ (from the neutral electrolyte). This trend agrees with the trend observed for the ionic conductivity of the three electrolytes, acidic>basic>neutral.[80] Comparing the two carbon

Table 4. Retention of the specific capacitance, in percentage, for the cations and anions deduced from comparison of the specific capacitance measured at 1 and 30 mA cm^{-2}. The results are for the original and heat-treated carbon cloth.

Electrode	H_3O^+	Na^+	K^+	HSO_4^-	SO_4^{2-}	OH^-
Original CC	76±2	51±6	57±3	64±3	41±5	--
Heat-treated CC	85±1	55±4	64±3	60±3	45±4	--

cloths, the capacitance retention of the cations is slightly higher for the heat-treated CC with lower content in surface oxygen groups and slightly broader micropores. The capacitance retention of the anions follows the trend HSO_4^- > SO_4^{2-} > OH^- (see also Figure 7). The lowest capacitance retention of the OH^- anion could be associated with its

larger size. Comparing the two carbon cloths, the capacitance retention of each anion is nearly the same. This suggests that the broadening of the micropores was not sufficient to mark differences. The comparison between the cation and anion of the same electrolyte shows that the capacitance retention is higher for the cation, with smaller electro-adsorbed size,[56,81-84] than for the anion. These results underline the dominance of the cations over the anions at the electric electrolyte/electrode interface also under dynamic conditions.

CONCLUSIONS

The total specific capacitance following the trend acidic > basic > neutral electrolyte is explained on the basis of the specific capacitance and the working potential windows associated with the cations and anions according to eq. (1). The specific capacitance associated with the cations follow the trend H_3O^+ > Na^+ or K^+ from basic electrolytes > Na^+ or K^+ from neutral electrolytes. Higher values are reached for the original carbon cloth, which has a higher content of surface oxygen groups. The specific capacitance associated with the anions follows the trend HSO_4^- > SO_4^{2-} > OH^-; the reached values are slightly higher for the heat-treated carbon cloth, with slightly larger specific surface area and broader microporosity. For the three aqueous electrolytes, the specific capacitance associated with the cation is higher than that associated with the anion.

The total working potential window following the trend neutral > acidic ≈ basic electrolyte is the sum of the working potential window measured for the cation and anion. The working potential window for the cations is similar for the three electrolytes and slightly broader for the original carbon cloth. The working potential windows for the anions follow the trend neutral > acidic ≥ basic electrolyte and are slightly broader

for the heat-treated carbon cloth. For each aqueous electrolyte, the working potential window associated with the cation is clearly broader than the one associated with the anion.

The charge stored by the cations and anions at the electric electrolyte/electrode interface has been deduced. The charge stored by the cations follows the trend H_3O^+>Na^+ or K^+ (from the basic electrolytes) > Na^+ or K^+ (from the neutral electrolytes); the charge is higher for the carbon cloth with higher content of surface oxygen groups. The charge stored by the anions follows the trend SO_4^{2-}>HSO_4^->OH^-; the charge is higher for the carbon cloth with slightly larger surface area and broader micropores. For each electrolyte, under stationary or dynamic conditions, the charge stored by the cations is much higher than that stored by the anions evidencing a dominance of the cations over the anions at the electric electrolyte/electrode interface. The dominance of the cations supports the suitability of the two carbon cloths as negative electrodes in asymmetric and hybrid supercapacitors.

SUPPORTING INFORMATION

Experimental results deal with: the potassium content deduced from EDS on the carbon fibers, the DFT pore size distributions for the two carbon cloths, fittings for determining the *PZC* values, CVs obtained at different potential scan rates and C_{2E} specific capacitances obtained from symmetric two-electrode cells.

ACKNOWLEDGEMENTS

Financial supports from the projects of reference MAT2014-57687-R and FCT-M-ERA-NET/0004/2014, PCIN-2015-024 are gratefully acknowledged. We thank J. A. Diaz from Carbongen SA and R. Beneito from AIJU for providing the original carbon cloth and also for helpful discussions about this material.

REFERENCES

(1) Rowlands, S. E.; Latham, R. J.; Schlindwein, W. S. Supercapacitor devices using porous silicon electrodes. *Ionics* **1999**, *5*, 144-149.
(2) Niu, J.; Pell, W.G.; Conway, B. E. Requirements for performance characterization of C double layer supercapacitors: Applications to a high specific-area C-cloth material. *J. Power Sources* **2006**, *156*, 725-740.
(3) Pandolfo, A. G.; Hollenkamp, A. F. Carbon properties and their role in supercapacitors. *J. Power Sources* **2006**, *157*, 11-27.
(4) Inagaki, M.; Konno, H.; Tanaike, O. Carbon materials for electrochemical capacitors. *J. Power Sources* **2010**, *195*, 7880-7903.
(5) Chmiola, J.; Largeot, C.; Taberna, P.-L.; Simon, P; Gogotsi, Y. Monolithic carbide-derived carbon films for micro-supercapacitors. *Science* **2010**, *328*, 480-483.
(6) Ghidiu, M.; Lukatskaya, M. R.; Zhao, M.-Q.; Gogotsi, Y.; Barsoum, M. W. Conductive two-dimensional titanium carbide clay with high volumetric capacitance. *Nature* **2014**, *516*, 78-81.
(7) Zhu, Y.; Stoller, M. D.; Cai, W.; Velamakanni, A.; Piner, R. D.; Chen, D.; Ruoff, R. S. Exfoliation of graphite oxide in propylene carbonate and thermal reduction of the resulting graphene oxide platelets. *ACS Nano* **2010**, *4*, 1227-1233.
(8) Yang, X.; Cheng, C.; Wang, Y.; Qiu, L.; Li, D. Liquid-mediated dense integration of graphene materials for compact capacitive energy storage. *Science* **2013**, *341*, 534-537.
(9) Li, H.; Tao, Y.; Zheng, X.; Li, Z.; Liu, D.; Xu, Z.; Luo, C.; Luo, J.; Kang, F.; Yang, Q.-H. Compressed porous graphene particles for use as supercapacitor electrodes with excellent volumetric performance. *Nanoscale* **2015**, *7*, 18459-18463.
(10) Li, H.; Tao, Y.; Zheng, X.; Luo, J.; Kang, F.; Cheng, H.-M.; Yang, Q.-H. Ultra-thick graphene bulk supercapacitor electrodes for compact energy storage. *Energy Environ. Sci.* **2016**, *9*, 3135-3142.
(11) Ma, C.; Song, Y.; Shi, J.; Zhang, D.; Zhong, M.; Guo, Q.; Liu, L. Phenolic-based carbon nanofiber webs prepared by electrospinning. *Mater. Lett.* **2012**, *76*, 211-214.
(12) Chen, Y.-C.; Hsu, Y.-K.; Lin, Y.-G.; Lin, Y.-K.; Horng, Y.-Y.; Chen, L.-C.; Chen, K.-H. Highly flexible supercapacitors with manganese oxide nanosheet/carbon cloth electrode. *Electrochim. Acta* **2011**, *56*, 7124-7130.
(13) Jost, K.; Stenger, D.; Perez, C.R.; McDonough, J.K.; Lian, K.; Gogotsi, Y; Dion, G. Knitted and screen printed carbon-fiber supercapacitors for applications in wearable electronics. *Energy Environ. Sci.* **2013**, *6*, 2698-2705.
(14) Bao, L.; Li, X. Towards textile energy storage from cotton T-shirts. *Adv. Mater.* **2012**, *24*, 3246-3252.
(15) Kou, L.; Huang, T.; Zheng, B.; Han, Y.; Zhao, X.; Gopalsamy, K.; Sun, H.; Gao, C. Coaxial wet-spun yarn supercapacitors for high-energy density and safe wearable electronics. *Nat. Commun.* **2014**, *5*, 3754.
(16) Zhang, T.; Kim, C. H. J.; Cheng, Y.; Ma, Y.; Zhang, H.; Liu, J. Making a commercial carbon fiber cloth having comparable capacitances to carbon nanotubes and graphene in supercapacitors through a top-down approach. *Nanoscale* **2015**, *7*, 3285-3291.
(17) Jiang, S.; Shi, T.; Zhan, X.; Long, H.; Xi, S.; Hu, H.; Tang, Z. High-performance all-solid-state flexible supercapacitors based on two-step activated carbon cloth. *J. Power Sources* **2014**, *272*, 16-23.

(18) Wang, G.; Wang, H.; Lu, X.; Ling, Y.; Yu, M.; Zhai, T.; Tong, Y.; Li, Y. Solid-state supercapacitor based on activated carbon cloths exhibits excellent rate capability. *Adv. Mater.* **2014**, *26*, 2676-2682.
(19) Wang, W.; Liu, W.; Zeng, Y.; Han, Y.; Yu, M.; Lu, X.; Tong, Y. A novel exfoliation strategy to significantly boost the energy storage capability of commercial carbon cloth. *Adv. Mater.* **2015**, *27*, 3572-3578.
(20) Ye, D.; Yu, Y.; Tang, J.; Liu, L.; Wu, Y. Electrochemical activation of carbon cloth in aqueous inorganic salt solution for superior capacitive performance. *Nanoscale* **2016**, *8*, 10406-10414.
(21) Gao, S.; Zhu, L.; Liu, L.; Gao, A.; Liao, F.; Shao, M. Improved energy storage performance based on gamma-ray irradiated activated carbon cloth. *Electrochim. Acta* **2016**, *191*, 908-915.
(22) Jiang, S.; Shi, T.; Zhan, X.; Huang, Y.; Tang, Z. Superior electrochemical performance of carbon cloth electrode-based supercapacitors through surface activation and nitrogen doping. *Ionics* **2016**, *22*, 1881-1890.
(23) Hsieh, C.-T.; Teng, H. Influence of oxygen treatment on electric double layer capacitance of activated carbon fabrics. *Carbon* **2002**, *40*, 667-674.
(24) Milczarek, G.; Ciszewski, A.; Stepniak, I. Oxygen-doped activated carbon fiber cloth as electrode material for electrochemical capacitor. *J. Power Sources* **2011**, *196*, 7882-7885.
(25) Shang, T. X.; Cai, X. X.; Jin, X. J. Phosphorus- and nitrogen-co-doped particleboard based activated carbon in supercapacitor application. *RSC Adv.* **2015**, *5*, 16433-16438.
(26) Geng, Y.; Song, Y.; Zhong, M.; Shi, J.; Guo, Q.; Liu, L. Influence of the pitch fluoride on the electrical conductivity of the activated carbon cloth as electrodes of supercapacitor. *Mater. Lett.* **2010**, *64*, 2673-2675.
(27) Wang, G.; Ling, Y.; Qian, F.; Yang, X.; Liu, X.-X.; Li, Y. Enhanced capacitance in partially exfoliated multi-walled carbon nanotubes. *J. Power Sources* **2011**, *196*, 5209-5214.
(28) Hsu, Y.-K.; Chen, Y.-C.; Lin, Y.-G.; Chen, L.-C.; Chen, K.-H. High-cell-voltage supercapacitor of carbon nanotube/carbon cloth operating in neutral aqueous solution. *J. Mater. Chem.* **2012**, *22*, 3383-3387.
(29) Du, J. X.; Mishra, D.; Ting, J.-M. Surface modified carbon cloth for use in electrochemical capacitor. *App. Surf. Sci.* **2013**, *285P*, 483-489.
(30) Wang, S.; Pei, B.; Zhao, X.; Dryfe, R. A. W. Highly porous graphene on carbon cloth as advanced electrodes for flexible all-solid-state supercapacitors. *Nano Energy* **2013**, *2*, 530-536.
(31) Wang, S.; Dryfe, R. A. W. Graphene oxide-assisted deposition of carbon nanotubes on carbon cloth as advanced binder-free electrodes for flexible supercapacitors. *J. Mater. Chem. A* **2013**, *1*, 5279-5283.
(32) Zhou, C.; Liu, J. Carbon nanotube network film directly grown on carbon cloth for high-performance solid-state flexible supercapacitors. *Nanotechnology* **2014**, *25*, 035402-035409.
(33) Zhou, Y.; Wang, S. Interconnecting carbon fibers with the in-situ electrochemically exfoliated graphene as advanced binder-free electrode materials for flexible supercapacitor. *Sci. Rep.* **2015**, *5*, 11792.
(34) Lei, C.; Markoulidis, F.; Wilson, P.; Lekakou, C. Phenolic carbon cloth-based electric double-layer capacitors with conductive interlayers and graphene coating. *J. Appl. Electrochem.* **2016**, *46*, 251-258.

(35) Wang, Y.; Tang, S.; Vongehr, S.; Syed, J. A.; Wang, X.; Meng, X. High-performance flexible solid-state carbon cloth supercapacitors based on highly processible N-graphene doped polyacrylic acid/polyaniline composites. *Sci. Rep.* **2016**, *6*, 12883.
(36) Horng, Y.-Y.; Lu, Y.-C.; Hsu, Y.-K.; Chen, C.-C.; Chen, L.-C.; Chen, K.-H. Flexible supercapacitor based on polyaniline nanowires/carbon cloth with both gravimetric and area-normalized capacitance. *J. Power Sources* **2010**, *195*, 4418-4422.
(37) Xu, J.; Wang, Q.; Wang, X.; Xiang, Q.; Liang, B.; Chen, D.; Shen, G. Flexible asymmetric supercapacitors based upon Co_9S_8 nanorod//Co_3O_4@RuO_2 nanosheet arrays on carbon cloth. *ACS Nano* **2013**, *7*, 5453-5462.
(38) Luan, F.; Wang, G.; Ling, Y.; Lu, X.; Wang, H.; Tong, Y.; Liu, X.-X.; Li, Y. High energy density asymmetric supercapacitors with a nickel oxide nanoflake cathode and a 3D reduced graphene oxide anode. *Nanoscale* **2013**, *5*, 7984-7990.
(39) Wang, Q.; Wang, X.; Liu, B.; Yu, G.; Hou, X.; Chen, D.; Shen, G. $NiCo_2O_4$ nanowire arrays supported on Ni foam for high-performance flexible all-solid-state. *J. Mater. Chem. A* **2013**, *1*, 2468-2473.
(40) Xiong, G.; Meng, C.; Reifenberger, R. G.; Irazoqui, P. P.; Fisher, T. S. Graphitic petal electrodes for all-solid-state flexible supercapacitors. *Adv. Energy Mater.* **2014**, *4*, 1300515.
(41) Zhang, Y.; Hu, Z.; Liang, Y.; Yang, Y.; An, N.; Li, Z.; Wu, H. Growth of 3D SnO_2 nanosheets on carbon cloth as a binder-free electrode for supercapacitors. *J. Mater. Chem. A* **2015**, *3*, 15057-15067.
(42) He, S.; Chen, W. Application of biomass-derived flexible carbon cloth coated with MnO_2 nanosheets in supercapacitors. *J. Power Sources* **2015**, *294*, 150-158.
(43) Pan, Z.; Qiu, Y.; Yang, J.; Ye, F.; Xu, Y.; Zhang, X.; Liu, M.; Zhang, Y. Ultra-endurance flexible all-solid-state asymmetric supercapacitors based on three-dimensionally coated MnOx nanosheets on nanoporous current collectors. *Nano Energy* **2016**, *26*, 610-619.
(44) Huang, Z.-H.; Song, Y.; Xu, X.-X.; Liu, X.-X. Ordered polypyrrole nanowire arrays grown on a carbon cloth substrate for high performance pseudocapacitor electrode. *ACS Appl. Mater. Interfaces* **2015**, *7*, 25506-25513.
(45) Nagaraju, G.; Ko, Y. H.; Yu, J .S. Tricobalt tetroxide nanoplate arrays on flexible conductive fabric substrate: Facile synthesis and application for electrochemical supercapacitors. *J. Power Sources* **2015**, *283*, 251-259.
(46) Sieben, J. M.; Morallon, E.; Cazorla-Amoros, D. Flexible ruthenium oxide-activated carbon cloth composites prepared by simple electrodeposition methods. *Energy* **2013**, *58*, 519-526.
(47) Aldama, I; Barranco, V.; Centeno, T. A.; Ibañez, J.; Rojo, J. M. Composite electrodes made from carbon cloth as supercapacitor material and manganese and cobalt oxide as battery one. *J. Electrochem. Soc.* **2016**, *163*, A758-A765.
(48) Chen, P.; Chen, H.; Qiu, J.; Zhou, C. Inkjet printing of single-walled carbon nanotube/RuO_2 nanowire supercapacitors on cloth fabrics and flexible substrates. *Nano Res.* **2010**, *3*, 594-603.
(49) Balducci, A.; Dugas, R.; Taberna, P. L.; Simon, P.; Plee, D.; Mastragostino, M.; Passerini, S. High temperature carbon-carbon supercapacitor using ionic liquid as electrolyte. *J. Power Sources* **2007**, *165*, 922-927.
(50) Hall, P. J.; Mirzaeian, M.; Fletcher, I.; Sillars, F. B.; Rennie, A. J. R.; Shiita-Bey, G. O.; Wilson, G.; Cruden, A.; Carter, R. Energy storage in electrochemical capacitors: designing functional materials to improve performance. *Energy Environ. Sci.* **2010**, *3*, 1238-1251.

(51) Lewandowski, A.; Olejniczak, A.; Galinski, M.; Stepniak, I. Performance of carbon-carbon supercapacitors based on organic, aqueous and ionic liquid electrolyte. *J. Power Sources* **2010**, *195*, 5814-5819.
(52) Sillars, F. B.; Fletcher, S. I.; Mirzaeian, M.: Hall, P. J. Effect of activated carbon xerogel pore size on the capacitance performance of ionic liquid electrolytes. *Energy Environ. Sci.* **2011**, *4*, 695-706.
(53) Vaquero, S.; Díaz, R.; Anderson, M.; Palma, J.; Marcilla, R. Insights into the influence of pore size distribution and surface functionalities in the behavior of carbon supercapacitors. *Electrochim. Acta* **2012**, *85*, 241-247.
(54) Kurig, H.; Vestli, M.; Tonurist, K.; Janes, A.; Lust, E. Influence of room temperature ionic liquid anion chemical composition and electrical charge delocalization on the supercapacitor properties. *J. Electrochem. Soc.* **2012**, *159*, A944-A951.
(55) Beguin, F.; Presser, V.; Balducci, A.; Frackowiak, E. Carbons and electrolytes for advanced supercapacitors. *Adv. Mater.* **2014**, *26*, 2219-2251.
(56) Eliad, L.; Salitra, G.; Soffer, A.; Aurbach, D. Ion sieving effects in the electrical double layer of porous carbon electrodes: Estimating effective ion size in electrolytic solutions. *J. Phys. Chem. B* **2001**, *105*, 6880-6887.
(57) Nian, Y.-R.; Teng, H. Nitric acid modification of activated carbon electrodes for improvement of electrochemical capacitance. *J. Electrochem. Soc.* **2002**, *149*, A1008-A1014.
(58) Hu, C.-C.; Wang, C.-C. Effects of electrolytes and electrochemical pretreatments on the capacitive characteristics of activated carbon fabrics for supercapacitors. *J. Power Sources* **2004**, *125*, 299-308.
(59) Babel, K.; Jurewicz, K. KOH activated carbon fabrics as supercapacitor material. *J. Phys. Chem. Solids* **2004**, *65*, 275-280.
(60) Toupin, M.; Belanger, D.; Hill, I. R.; Quinn, D. Performance of experimental carbon blacks in aqueous supercapacitors. *J. Power Sources* **2005**, *140*, 203-210.
(61) Andreas, H. A.; Conway, B. E. Examination of the double layer capacitance of a high specific-area C-cloth electrode titrated from acidic to alkaline pHs. *Electrochim. Acta* **2006**, *51*, 6510-6520.
(62) Beguin, F.; Friebe, M.; Jurewicz, K.; Vix-Gurtel, C.; Dentzer, J.; Frackowiak, E. State of hydrogen electrochemically stored using nanoporous carbons as negative electrode materials in an aqueous medium. *Carbon* **2006**, *44*, 2392-2398.
(63) Ruiz, V.; Blanco, C.; Raymundo-Piñero, E.; Khomenko, V.; Beguin, F.; Santamaria, R. Effects of thermal treatment of activated carbon on the electrochemical behavior in supercapacitors. *Electrochim. Acta* **2007**, *52*, 4969-4973.
(64) Subramanian, V.; Luo, C.; Stephan, A. M.; Nahm, K. S.; Thomas, S.; Wei, B. Supercapacitors from activated carbon derived from banana fibers. *J. Phys. Chem. C* **2007**, *111*, 7527-7531.
(65) Qu, Q. T.; Wang, B.; Yang, L. C.; Shi, Y.; Tian, S.; Wu, Y. P. Study on electrochemical performance of activated carbon in aqueous Li_2SO_4, Na_2SO_4 and K_2SO_4 electrolytes. *Electrochem. Commun.* **2008**, *10*, 1652-1655.
(66) Demarconnay, L.; Raymundo-Piñero, E.; Beguin, F. A symmetric carbon/carbon supercapacitor operating at 1.6 V by using a neutral aqueous solution. *Electrochem. Commun.* **2010**, *12*, 1275-1278.
(67) Bichat, M. P.; Raymundo-Piñero, E.; Beguin, F. High voltage supercapacitor built with seaweed carbons in neutral aqueous electrolyte. *Carbon* **2010**, *48*, 4351-4361.

(68) Stepniak, I.; Ciszewski, A. New design of electric double layer capacitors with aqueous LiOH electrolyte as alternative to capacitors with KOH solution. *J. Power Sources* **2010**, *195*, 2564-2569.
(69) Yin, J.; Zheng, C.; Qi, L.; Wang, H. Concentrated $NaClO_4$ aqueous solutions as promising electrolytes for electric double-layer capacitors. *J. Power Sources* **2011**, *196*, 4080-4087.
(70) Fic, K.; Lota, G.; Meller, M.; Frackowiak, E. Novel insight into neutral medium as electrolyte for high-voltage supercapacitors. *Energy Environ. Sci.* **2012**, *5*, 5842-5850.
(71) Staiti, P.; Arenillas, A.; Lufrano, F.; Menendez, J. A. High energy ultracapcitor based on carbon xerogel electrodes and sodium sulfate electrolyte. *J. Power Sources* **2012**, *214*, 137-141.
(72) Volfkovich, Y. M.; Bograchev, D. A.; Mikhalin, A. A.; Bagotsky, V. S. Supercapacitor carbon electrodes with high capacitance. *J. Solid. State Electrochem.* **2014**, *18*, 1351-1363.
(73) Okajima, K.; Ohta, K.; Sudoh, M. Capacitance behavior of activated carbon fibers with oxygen-plasma treatment. *Electrochim. Acta* **2005**, *50*, 2227-2231.
(74) Soneda, Y.; Yamashita, J.; Kodama, M.; Hatori, H.; Toyoda, M.; Inagaki, M. Pseudo capacitance on exfoliated carbon fiber in sulfuric acid electrolyte. *Appl. Phys. A* **2006**, *82*, 575-578.
(75) Centeno, T. A.; Hahn, M.; Fernandez, J. A.; Kotz, R.; Stoeckli, F. Correlation between capacitance of porous carbons in acidic and aprotic EDLC electrolytes. *Electrochem. Commun.* **2007**, *9*, 1242-1246.
(76) Barranco, V.; Lillo-Rodenas, M. A.; Linares-Solano, A.; Oya, A.; Pico, F.; Ibañez, J.; Agullo-Rueda, F.; Amarilla, J. M.; Rojo, J. M. Amorphous carbon nanofibers and their activated carbon nanofibers as supercapacitor electrodes. *J. Phys. Chem. C* **2010**, *114*, 10302-10307.
(77) Levi, M. D.; Salitra, G.; Mevy, N.; Aurbach, D.; Maier, J. Application of a quartz-crystal microbalance to measure ionic fluxes in microporous carbons for energy storage. *Nature Mater.* **2009**, *8*, 872-875.
(78) Shao, L.-H.; Biener, J.; Kramer, D.; Viswanath, R. N.; Baumann, T. F.; Hamza, A. V.; Weissmuller, J. Electrocapillary maximum and potential of zero charge of carbon aerogel. *Phys. Chem. Chem. Phys.* **2010**, *12*, 7580-7587.
(79) Zebardast, H. R.; Rogak, S.; Asselin, E. Potential of zero charge of glassy carbon at elevated temperatures. *J. Electroanal. Chem.* **2014**, *724*, 36-42.
(80) *Handbook of Chemistry and Physics*. Lide, D. R. Ed.; Taylor and Francis Group 88th Edition. Boca Raton 2007-2008. Pp 5-72 and pp 15-29.
(81) Eliad, L.; Salitra, G.; Soffer, A.; Aurbach, D. Proton selective environment in the pores of activated molecular sieving carbon electrodes. *J. Phys. Chem. B* **2002**, *106*, 10128-10134.
(82) Ruiz, V.; Blanco, C.; Santamaria, R.; Juarez-Galan, J. M.; Sepulveda-Escribano, A.; Rodriguez-Reinoso, F. Carbon molecular sieves as model active electrode materials in supercapacitors. *Micropores Mesopores Mater*. **2008**, *110*, 431-435.
(83) Garcia-Gomez, A.; Barranco, V.; Moreno-Fernandez, G.; Ibañez, J.; Centeno, T. A.; Rojo, J. M.. Correlation between capacitance and porosity in microporous carbon monoliths. *J. Phys. Chem. C* **2014**, *118*, 5134-5141.
(84) Moreno-Fernandez, G.; Kunowsky, M.; Lillo-Rodenas, M. A.; Ibañez, J.; Rojo, J. M. New carbon monoliths for supercapacitor electrodes. Looking at the double layer. *ChemElectroChem* DOI: 10.1002/celc.201600848.

TOC Graphic

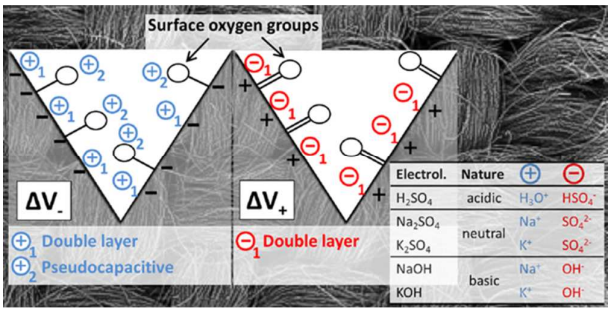
Surface oxygen groups
ΔV-
ΔV+
Double layer
Pseudocapacitive
Double layer
Electrol.
Nature
H2SO4
acidic
H3O+
HSO4-
Na2SO4
K2SO4
neutral
Na+
K+
SO4 2-
SO4 2-
NaOH
KOH
basic
Na+
K+
OH-
OH-

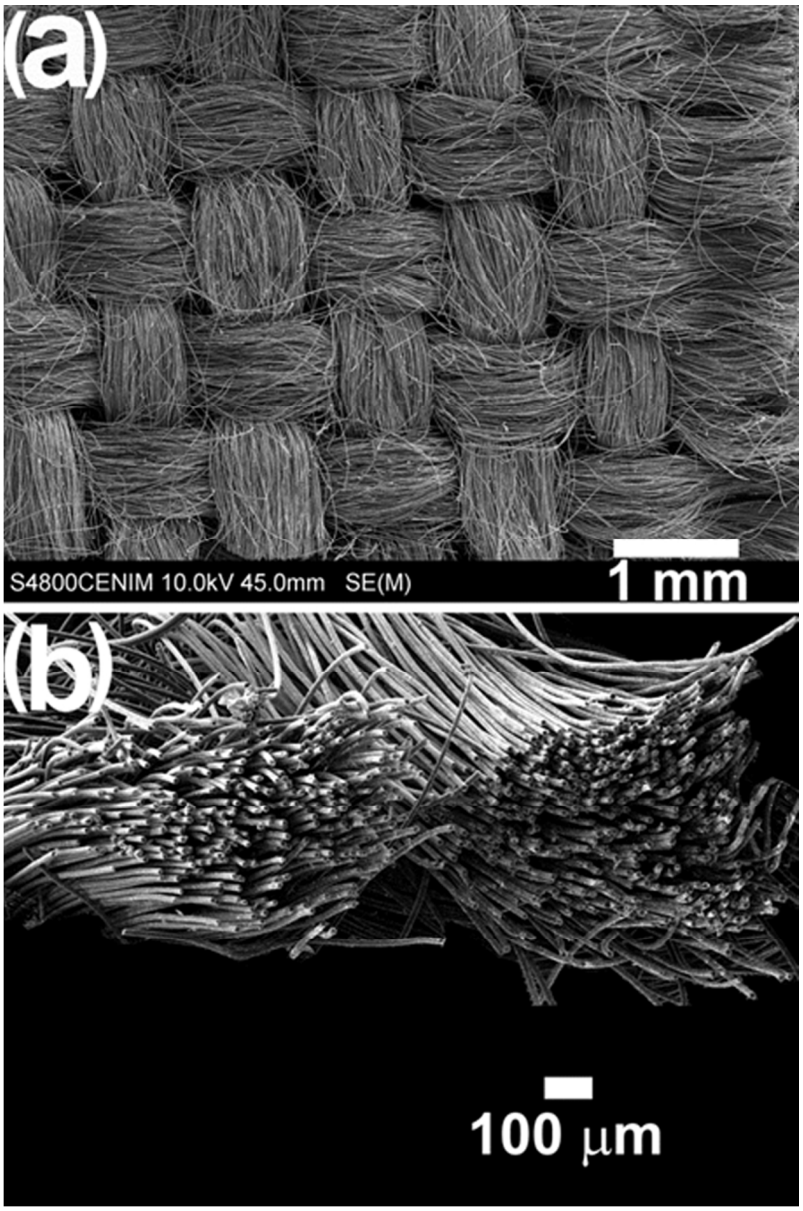

Figure 1. SEM pictures showing a piece of the original carbon cloth (a) and two threads consisting of bundles of carbon fibers (b).

70x105mm (300 x 300 DPI)

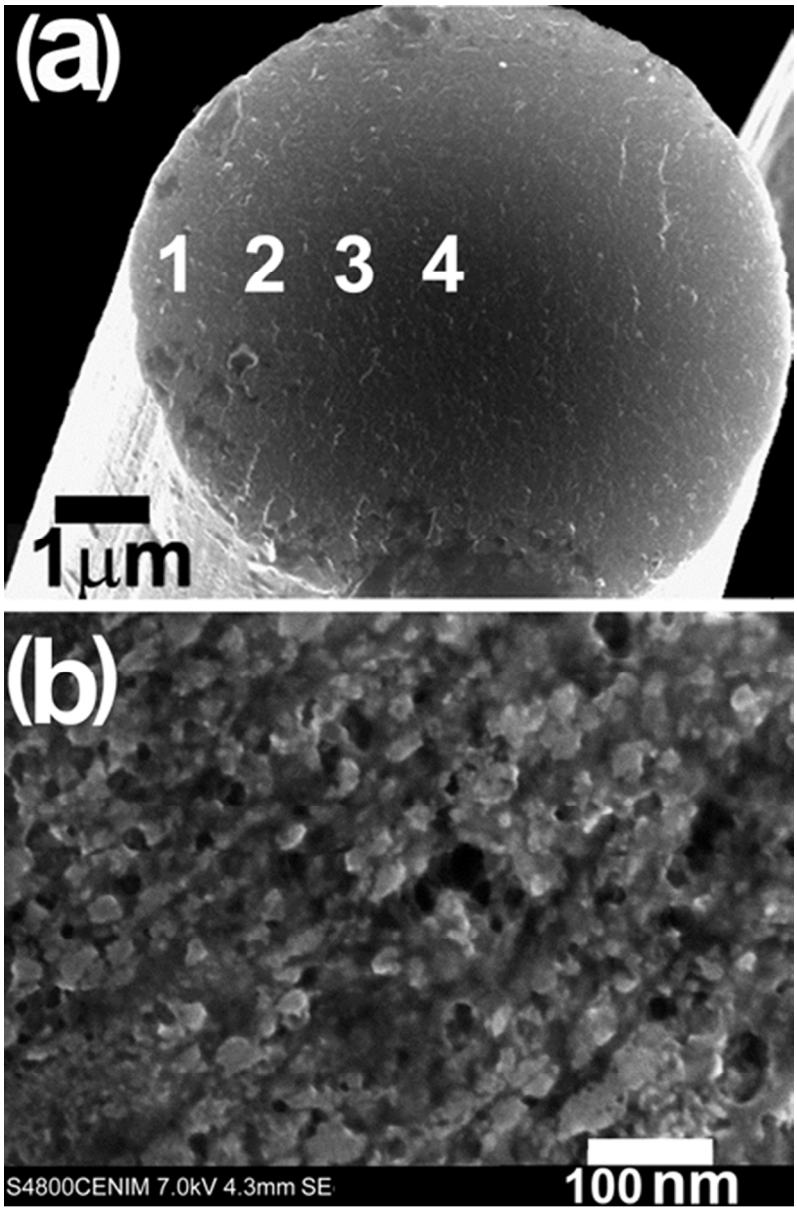

Figure 2. SEM picture of the section of a carbon fiber (a) and a magnified picture of that section (b).

70x106mm (300 x 300 DPI)

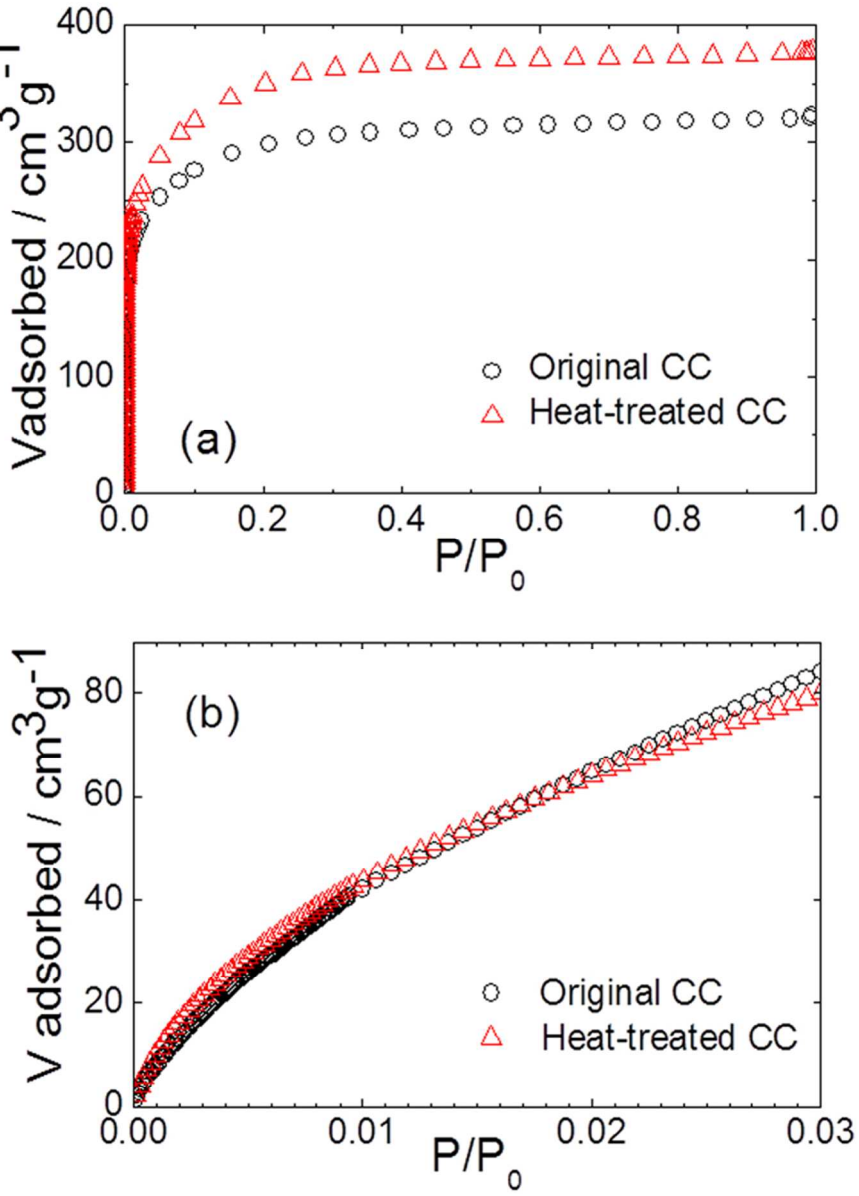

Figure 3. N2 (a) and CO2 (b) adsorption isotherms of the original (circles) and heat-treated (triangles) CC.

69x93mm (300 x 300 DPI)

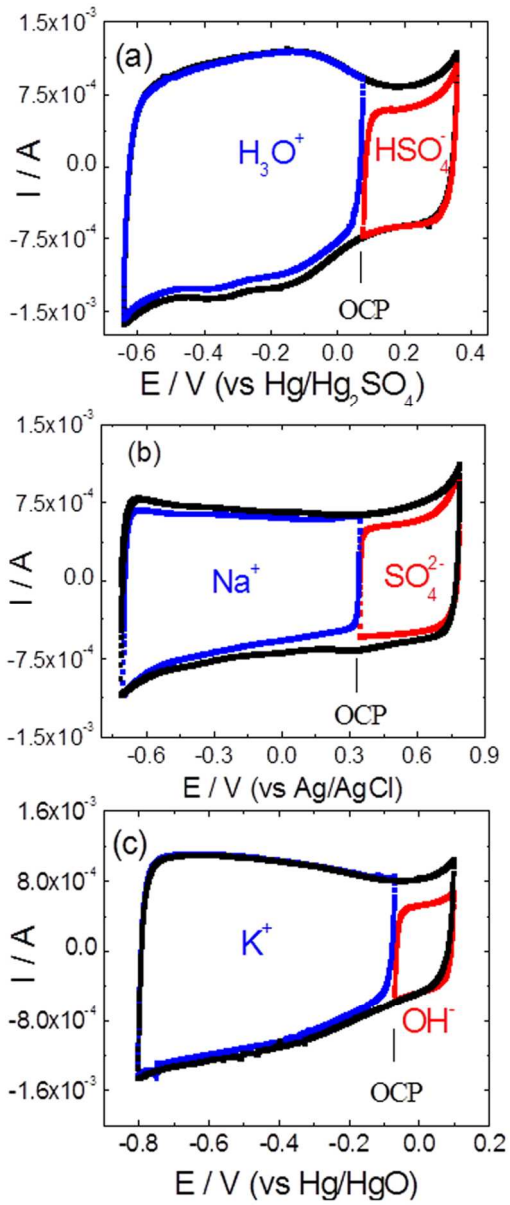

Figure 4. Cyclic voltammetries recorded for the electrolytes: H2SO4 (a), Na2SO4 (b) and KOH (c) on the original CC. The voltage scan rate was 0.5 mV s-1.

60x140mm (300 x 300 DPI)

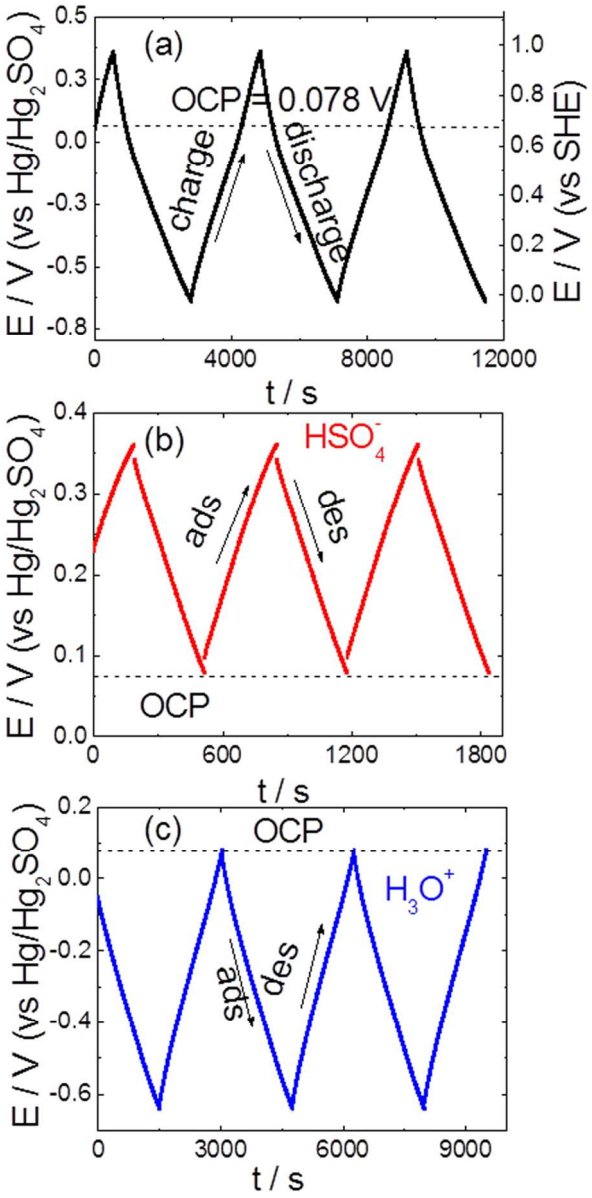

Figure 5. Galvanostatic charge/discharge plots recorded for the sulfuric acid electrolyte on the original CC in the total voltage range (a) and in the partial voltage ranges from the OCP to positive voltages (b) and to negative ones (c). The three plots were obtained at 1 mA cm-2.

70x140mm (300 x 300 DPI)

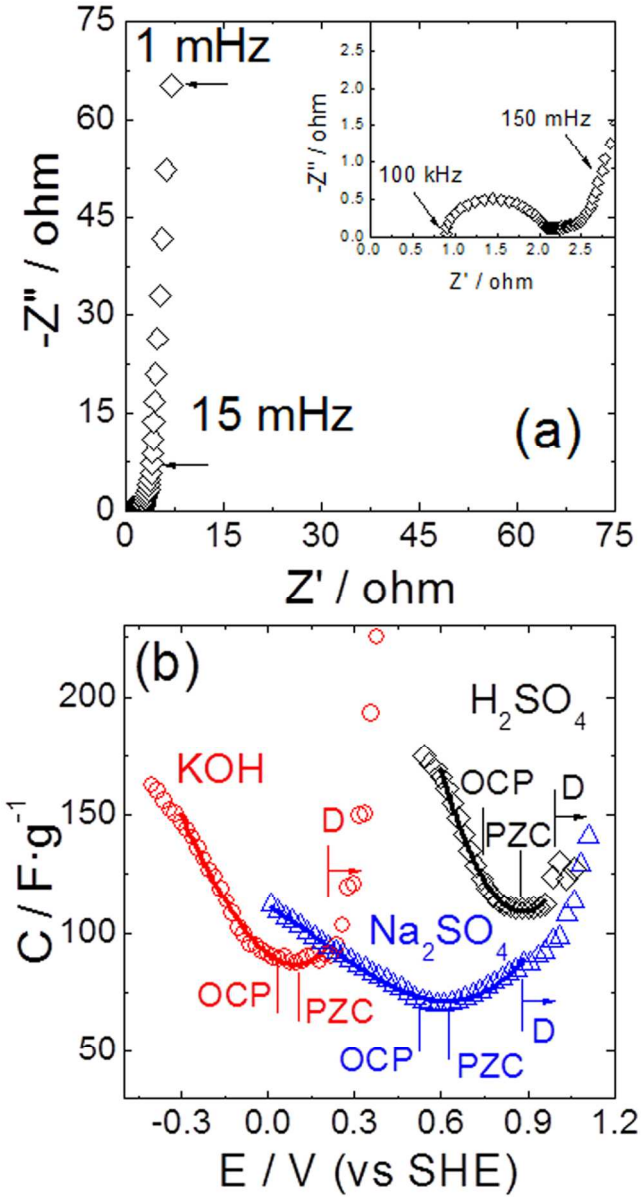

Figure 6. (a) Impedance plot recorded for the H2SO4 electrolyte at the OCP value on the original CC. Inset: the magnified plot obtained at higher frequencies. (b) Variation of the specific capacitance measured at 1 mHz vs. the potential for three electrolytes, KOH, Na2SO4 and H2SO4, in presence of the original CC. Solid lines are the best fittings for determining the PZC.

150x281mm (600 x 600 DPI)

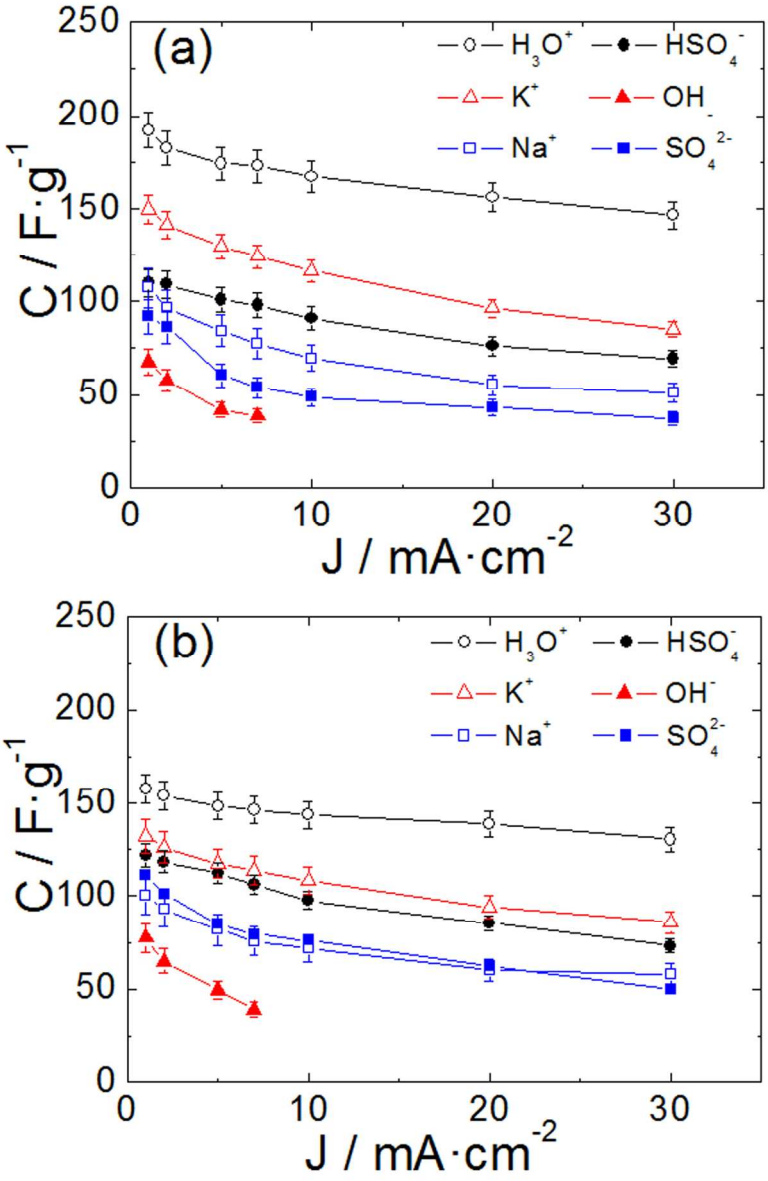

Figure 7. Dependence of the specific capacitance associated with the cations and anions of the electrolytes H2SO4, Na2SO4 and KOH as a function of the current density for the original (a) and heat-treated (b) CC.

112x169mm (600 x 600 DPI)

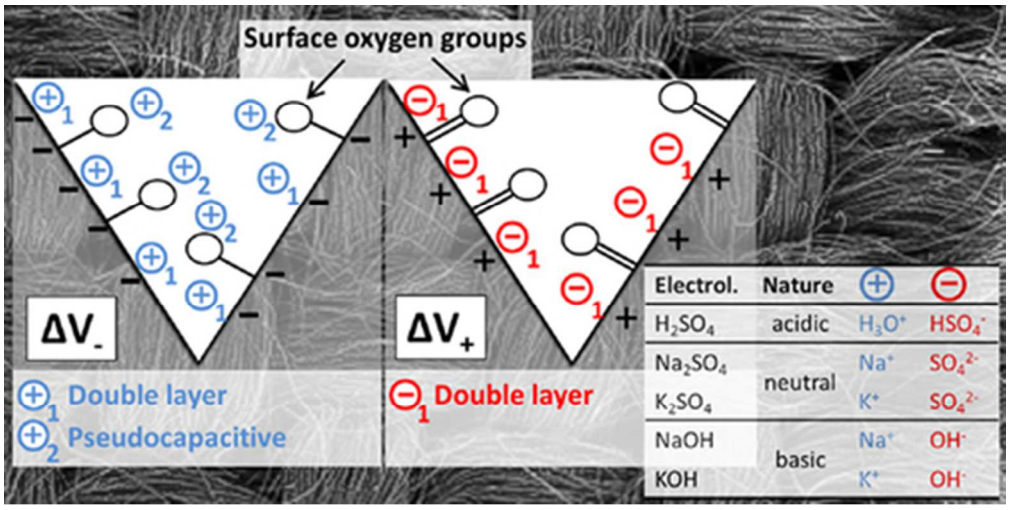

42x21mm (300 x 300 DPI)